

Physics-Based Prediction of Atmospheric Transfer Characteristics at Terahertz Frequencies

Xiaoyu He and Xiaojian Xu^{ID}

Abstract—The amplitude and phase distortions of radar echo signal will cause the emergence of undesirable ghost scattering points, which degrade the quality of terahertz (THz) radar images. In this paper, a physics-based procedure is presented to predict the atmospheric attenuation and dispersion characteristics at THz frequencies, which is mainly based on the line-by-line calculation method with a specific modification in phase-shift prediction. The line-by-line parameters provided by the high-resolution transmission spectroscopic database and atmospheric condition parameters obtained from the Air Force Geophysics Laboratory reference atmospheric constituent profiles are adopted to predict the atmospheric transmittance and the phase shift for specific transfer paths. The results are compared with measured data to demonstrate the accuracy, while the proposed procedure is used to analyze the impacts of atmospheric transfer characteristics on radar imaging via the high-resolution range profile simulation. The signal distortion is interpreted in terms of paired echoes to illustrate the importance of frequency band selection for high-resolution imagery at THz frequencies.

Index Terms—Atmospheric absorption, atmospheric dispersion, paired echoes, radio wave propagation, terahertz (THz).

I. INTRODUCTION

WITH the development of technology in remote sensing, there is an increased interest in the potential application of terahertz (THz) frequencies for radar imaging. THz systems, operating at frequencies between the millimeter waves and the far infrared (i.e., spectrum ranging from 0.1 to 10 THz), are expected to include various merits, such as wide bandwidths and penetrability [1]–[4]. As the THz frequencies are sensitive to water vapor, the THz systems are usually used in target detection at close and standoff distances instead of remote sensing at a long distance [5]–[8]. However, due to the fact that the water vapor in the earth atmosphere mainly distributed in the troposphere from the sea level to the altitude of 10 km, the THz systems can be potentially applied to aircraft detection at high latitude region.

To explore the mentioned applicability of THz systems, it is necessary for atmospheric radiative transfer characteristics in THz spectrum to be quantitatively studied and calibrated. Since most THz radar images are generated based on the

Manuscript received January 30, 2018; revised January 31, 2019; accepted February 19, 2019. Date of publication March 1, 2019; date of current version April 5, 2019. (Corresponding author: Xiaojian Xu.)

The authors are with the School of Electronic and Information Engineering, Beihang University, Beijing 100191, China (e-mail: xiaojianxu@buaa.edu.cn).

Color versions of one or more of the figures in this paper are available online at <http://ieeexplore.ieee.org>.

Digital Object Identifier 10.1109/TAP.2019.2902423

range-Doppler principle where reference phases were involved in imagery, both attenuation and phase shift caused by atmospheric propagation are considered. Based on the measured data and by curve fitting, several empirical models have been developed to predict the attenuations caused by atmospheric gases [9], rain [10], and clouds and fog [11] in spectrum from 0 to 1 THz. Necessary data have been obtained by the advanced THz spectroscopy system to analyze attenuation and phase shift [12], [13] in the spectrum ranging from 0.2 to 2 THz. However, scarce data and studies are available for the spectrum spanning from 2 to 10 THz.

The study of the atmospheric transfer characteristics at the THz frequencies largely focuses on water content [9]–[13]. Nevertheless, the earth atmosphere is a complex mixture involving various gases, while the vertical distribution of each gas is different to the others. To understand the impacts of atmospheric constituents on the attenuation and the phase shift of the transmitted signal, atmospheric constituent profiles [14] should be adopted in the analyses of the atmospheric characteristics for transfer paths at different altitudes.

In the infrared spectrum, six types of reference atmospheric constituent profiles [14] have been widely used to calculate transmittance and path radiance. A number of atmospheric radiative transfer models are developed and revised, such as the line-by-line radiative transfer model [15], the Moderate Resolution Transmission [16], and the Santa Barbara DISORT Atmospheric Radiative Transfer [17]. Although the frequency of THz is lower than the infrared, there is a possibility that the calculation methods in the developed models can be used to calculate atmospheric transmittance at the THz frequencies. Meanwhile, according to the infrared radiative theory [18], the path radiance is out of consideration at the THz frequencies since the emitted and scattered radiances from the earth atmosphere are extremely weak. The main demerit of using the developed model directly is the lack of calculation for phase shift caused by atmospheric propagation, as infrared and visible imaging sensors use focal plane arrays to acquire the magnitudes of spatial objects without the requirement of reference phases.

Illuminated by the calculation of atmospheric radiative transfer characteristics in the infrared, we aim at developing a physics-based model to quantitatively predict dispersive atmospheric transmittance and phase shift at the THz frequencies for radar imaging. The equations based on the line-by-line calculation method [15], [19] are deduced with

a specific modification in phase-shift prediction. For specific transfer paths at different altitudes, the atmospheric condition parameters from the Air Force Geophysics Laboratory (AFGL) reference atmospheric constituent profiles [14] and the line-by-line spectroscopic parameters in the high-resolution transmission (HITRAN) database [20] are adopted to calculate the absorption and the phase-shift coefficients for simulating high-resolution range profiles.

The remainder of this paper is organized as follows. The calculation for atmospheric transmittance and phase shift at the THz frequencies is discussed in Section II, where the equations based on the line-by-line calculation method are deduced to calculate attenuation as well as phase shift. In Section III, the calculated results are compared with the measured data to demonstrate accuracy, while the simulated range profiles are given to analyze the impacts of atmospheric transfer characteristics on radar imaging at the THz frequencies. Section IV provides the conclusion.

II. CALCULATION OF TRANSMITTANCE AND PHASE SHIFT

After atmospheric propagation, the transmitted signal can be presented in the frequency domain as

$$E(f, l) = E(f, 0) \cdot \tau(f, l) \cdot \exp[j\varphi(f, l)] \quad (1)$$

where E represents the THz signal, f denotes the signal frequency, l is the transfer distance, j represents the imaginary symbol, τ is the amplitude transmittance, which characterizes the attenuation of the signal amplitude, and φ denotes the total phase shift related to the atmospheric dispersion.

As it can be seen from (1), the impacts of the atmospheric transfer characteristics on the THz signal are related to the signal frequency as well as the transfer distance. Meanwhile, the attenuation and the phase shift of the signal can be considered separately, which are, respectively, detailed in Sections II-A and II-B.

A. Calculation of Absorption Attenuation

The transmittance in the infrared radiative transfer calculation is generally used to characterize the attenuation of the signal power instead of the signal amplitude [15]–[17]. Since the earth atmosphere is an inhomogeneous medium, the absorption characteristic can be different along the transfer path. Curtis–Godson assumption [21], [22] is adopted to simplify the calculation, where the inhomogeneous atmosphere is divided into a number of homogeneous layers. Then, the power transmittance can be expressed as

$$\tau'(f) = \exp \left[-\sum_{i=1}^L (k_e^{(i)}(f) \cdot l^{(i)}) \right] \quad (2)$$

where τ' denotes the spectral transmittance of power, $k_e^{(i)}$ is the spectral extinction coefficient in the i th layer, $l^{(i)}$ represents the transfer path length in the i th layer, and L is the total number of the transmitted atmospheric layers.

As the power of the signal is the square of its amplitude, the amplitude transmittance in (1) can be calculated as

$$\tau(f) = \exp \left[-0.5 \cdot \sum_{i=1}^L (k_e^{(i)}(f) \cdot l^{(i)}) \right]. \quad (3)$$

According to the infrared radiative transfer theory, the extinction coefficient k_e consists of spectral absorption coefficient and spectral scattering coefficient. However, since the scattering coefficient is negligible at the THz frequencies, only the absorption coefficient will be considered in the following discussion.

According to the line-by-line calculation method, the absorption coefficient can be calculated via accumulating the contribution of all spectral lines. As the scattering coefficient is ignored, the extinction coefficient in the i th layer is defined as

$$k_e^{(i)}(f) = \sum_{m=1}^M \left[N_m^{(i)} \cdot \frac{S_m(f_m)}{\pi} \cdot F_m(f, f_m, \Delta f_m) \right] \quad (4)$$

where M is the total number of spectral lines; $N_m^{(i)}$ denotes the number density of the absorbing molecule for the m th spectral line, in units of molecules \cdot cm $^{-3}$; S_m represents the line intensity of the m th spectral line, in units of Hz \cdot molecule $^{-1} \cdot$ cm 2 ; f_m and Δf_m are the transition frequency and the half-width of the m th spectral line, respectively; and F_m is the line shape function, which is assumed as the full-Lorentz profile in the infrared [23] and the Van Vleck–Weisskopf (VVW) profile in the microwave [24], that is,

$$F_m^{(L)}(f, f_m, \Delta f_m) = \frac{f}{f_m} \left[\frac{\Delta f_m}{(f - f_m)^2 + \Delta f_m^2} - \frac{\Delta f_m}{(f + f_m)^2 + \Delta f_m^2} \right] \quad (5)$$

$$F_m^{(V)}(f, f_m, \Delta f_m) = \frac{f^2}{f_m^2} \left[\frac{\Delta f_m}{(f - f_m)^2 + \Delta f_m^2} + \frac{\Delta f_m}{(f + f_m)^2 + \Delta f_m^2} \right] \quad (6)$$

where $F_m^{(L)}$ is the full-Lorentz profile, while $F_m^{(V)}$ is the VVW profile.

It should be noted that the second term in the square brackets of (5) and (6) are negligible at high frequency. In this case, the line shape function can be replaced with the Lorentz profile [19] for simplification.

The spectral line parameters, including S_m , f_m , and Δf_m , are generally obtained by means of measurement. The spectral line parameters provided by the HITRAN molecular spectroscopic database are used in the calculation. Since the data in the HITRAN database are in units of cm $^{-1}$, the amplitude transmittance in (3) is in units of cm $^{-1}$.

With the reference atmospheric constituent profiles [14], the number density of the absorbing molecule in the i th layer can be expressed as

$$N_m^{(i)} = p_m^{(i)} \cdot N^{(i)} \quad (7)$$

where $p_m^{(i)}$ is the mixing ratio of the absorbing molecule for the m th spectral line and $N^{(i)}$ is the molecular density of the atmosphere in units of molecules \cdot cm $^{-3}$, which is related to atmospheric temperature and pressure, given as

$$N^{(i)} = P^{(i)} / (k_B T^{(i)}) \quad (8)$$

where $P^{(i)}$ and $T^{(i)}$ are, respectively, the pressure and the temperature in the i th atmospheric layer, while k_B is Boltzmann's constant.

B. Calculation of Phase Shift

Similar to the amplitude transmittance, the total phase shift φ defined in (1) can also be defined with a coefficient and the transfer path length, that is,

$$\varphi = \sum_{i=1}^n (\beta^{(i)}(f) \cdot l^{(i)}) \quad (9)$$

where $\beta^{(i)}$ denotes the phase-shift coefficient in the i th layer, which can be defined as

$$\beta^{(i)}(f) = \frac{2\pi f}{c} [n^{(i)}(f) - 1] \quad (10)$$

where $n^{(i)}$ is the complex refractive index in the i th layer, subject to relative permittivity and relative permeability, and c denotes the propagation speed of electromagnetic wave. In the atmosphere, as the relative permeability approximate one, the complex refractive index can be written as

$$n^{(i)}(f) = \sqrt{\varepsilon_r^{(i)}(f)} \quad (11)$$

where $\varepsilon_r^{(i)}$ is the relative permittivity in the i th layer.

For the earth atmosphere, since the complex refractive index of the air is close to 1, $(n+1)/2$ is a negligible term which can be added into the following equation to simplify the equation, that is,

$$\beta^{(i)}(f) = \frac{\pi f}{c} [\varepsilon_r^{(i)}(f) - 1]. \quad (12)$$

The calculation of the dielectric constant has been discussed in [24, Sec. 13-3], where the equation with the VVW profile is given. Then, the phase-shift coefficient varying with frequency can be expressed as

$$\beta^{(i)}(f) = \sum_{m=1}^M \left[N_m^{(i)} \cdot \frac{S_m(f_m)}{\pi} \cdot f \cdot g_m(f, f_m, \Delta f_m) \right] \quad (13)$$

with

$$\begin{aligned} g_m(f, f_m, \Delta f_m) &= \frac{1}{f_m^2 - f^2} \cdot \left\{ 1 - \frac{f \cdot \Delta f_m^2}{2f_m^2} \left[\frac{f_m + f}{(f - f_m)^2 + \Delta f_m^2} \right. \right. \\ &\quad \left. \left. + \frac{f - f_m}{(f + f_m)^2 + \Delta f_m^2} \right] \right\} \end{aligned} \quad (14)$$

where g_m is a function related to the spectral line parameters.

Considering the function g_m defined in (14) is not zero at the frequency $f = 0$, the phase-shift coefficient in (13) is adjusted with an extra term to ensure the continuity of the phase-shift coefficient, that is,

$$\beta^{(i)}(f) = \sum_{m=1}^M \left\{ N_m^{(i)} \cdot \frac{S_m(f_m)}{\pi} \cdot f \cdot \left[g_m(f, f_m, \Delta f_m) - \frac{1}{f_m^2} \right] \right\}. \quad (15)$$

Note that the phase-shift coefficient is in units of $\text{rad} \cdot \text{cm}^{-1}$.

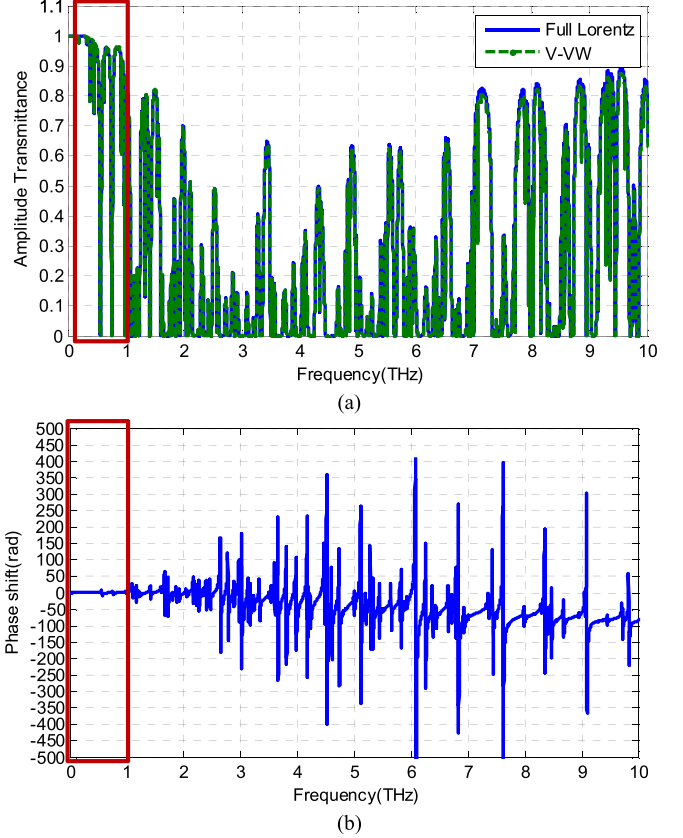


Fig. 1. Atmospheric characteristics through 6.18 m at temperature 21 °C with RH 51% from 0 to 10 THz. (a) Amplitude transmittance. (b) Phase shift.

III. EXAMPLES AND ANALYSIS

A. Validation

To validate the accuracy and the usefulness of the proposed approach, the calculated curves of amplitude transmittance and phase shift are compared with the measured data presented in [12] and [13]. Only the spectral lines of water vapor are considered in the calculation to improve efficiency.

In [12], the amplitude transmission through 6.18 m was measured at the temperature of 21 °C with the relative humidity (RH) of 51%, where the corresponding mass density of water vapor was $9.25 \text{ g} \cdot \text{m}^{-3}$.

To ensure a set of similar atmospheric conditions, we assume that the transfer path locates at the altitude of 1.01 km in the midlatitude summer atmosphere, where the corresponding mass density of water vapor is about $9.26 \text{ g} \cdot \text{m}^{-3}$.

Fig. 1 shows the calculated curves of the amplitude transmittance and the phase shift from 0 to 10 THz. Then, the calculated curves are truncated for spectrum spanning from 0.2 to 1.0 THz to compare with the measured data, as shown, respectively, in Figs. 2 and 3, where Figs. 2(a) and 3(a) show the measured data while Figs. 2(b) and 3(b) show the curves predicted by the proposed approach.

Fig. 2 presents the result in the spectral region from 0.2 to 1 THz. As it can be seen, the measured and the calculated curves show the same trend of variation, whereas the calculated amplitude transmittance is a little higher in

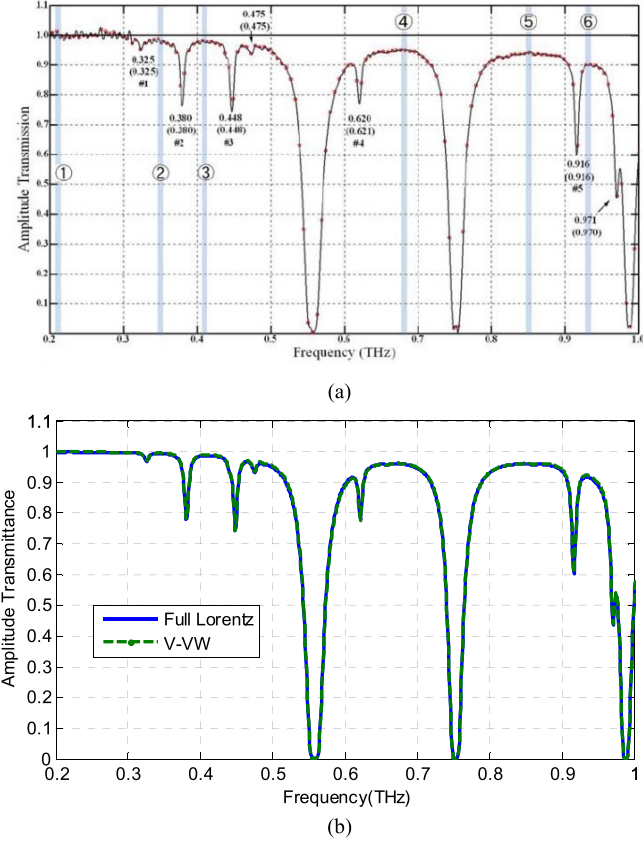


Fig. 2. Amplitude transmittance through 6.18 m of atmosphere at temperature 21 °C with RH 51% from 0.2 to 1 THz. (a) Measured [12]. (b) Calculated.

the atmospheric windows, such as 0.6–0.7 and 0.8–0.9 THz. In addition, there is a slight difference for the curves obtained using the full-Lorentz and the VVW profiles.

The phase shift through 6.18 m of atmosphere at temperature 21 °C with RH 51% from 0 to 1.1 THz is shown in Fig. 3. Fig. 3(a) is the figure given in [13], in Fig. 3(a) the black dots are the experimental data, whereas the red curve denotes the fitting result. Fig. 3(b) shows the curve calculated using (15). As it can be seen, the trend and the amplitude of the calculated curve are similar to the measured data. The location of the local maximal phase shift corresponds to the transition frequency of water vapor, while the phase shift seems to increase at higher frequency.

B. Prediction

The frequency-variant atmospheric transmittance and phase shift will lead to the amplitude and phase distortion of signals, which has dramatic impacts on radar imaging. Fig. 4 shows the atmospheric transfer characteristics and the simulated range profiles for a single scattering center at the frequency spanning from 466 to 481 GHz. The frequency channel is arbitrarily selected, while the scattering center is placed at 61 m, i.e., the atmospheric transfer distance is 122 m. The atmospheric condition in Section III-A is used to calculate atmospheric transmittance and phase shift. The ideal range profile and the profiles distorted by atmospheric propagation are shown

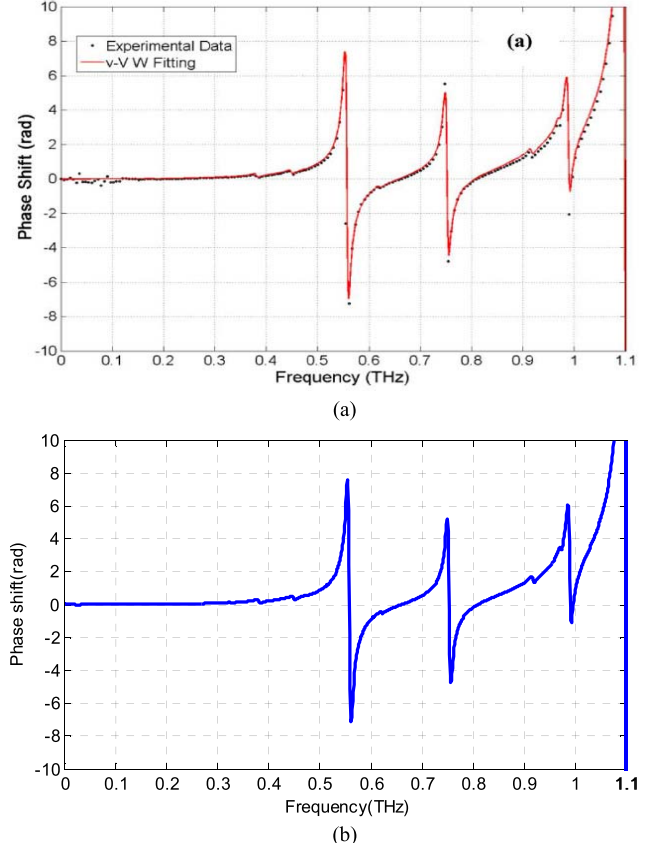


Fig. 3. Phase shift through 6.18 m of atmosphere at temperature 21 °C with RH 51% from 0 to 1.1 THz. (a) Measured [13]. (b) Calculated.

in Fig. 4(b) and (c), respectively, where the theoretical resolution with a rectangular window is 1 cm for 15 GHz bandwidth.

The amplitude and phase distortion of signals can be interpreted by means of the paired echoes [25]. For amplitude distortion, the average amplitude transmittance is about 0.4 shown in Fig. 4(a), while the transmittance is not a constant in the selected frequency channel. As the transmittance curve has a pit around about 475 GHz, a narrower main lobe and higher sidelobes can be observed in the range profile as shown by the blue curve in Fig. 4(c).

Regarding the phase distortion, since the phase shift increases with the frequency in the selected channel, an extra linear increase of phase can lead to the location shift of the scattering center, which can be expressed as

$$\Delta l = \frac{a_0 \cdot c}{2\pi} \quad (16)$$

where Δl is the shift distance, a_0 represents the approximate slope of the phase-shift curve, and c denotes the propagation speed of electromagnetic wave.

In Fig. 4(a), the approximate slope of the phase shift is about $1.3e^{-10}$ leading to the location shift of 0.6 cm. Since the range resolution is 1 cm for the bandwidth of 15 GHz, the peak of the range profile shifts from the set range, as shown by the green dashed curve in Fig. 4(c). In addition, as the phase shift increases nonlinearly with the frequency, at least two asymmetry pairs of echoes can be seen.

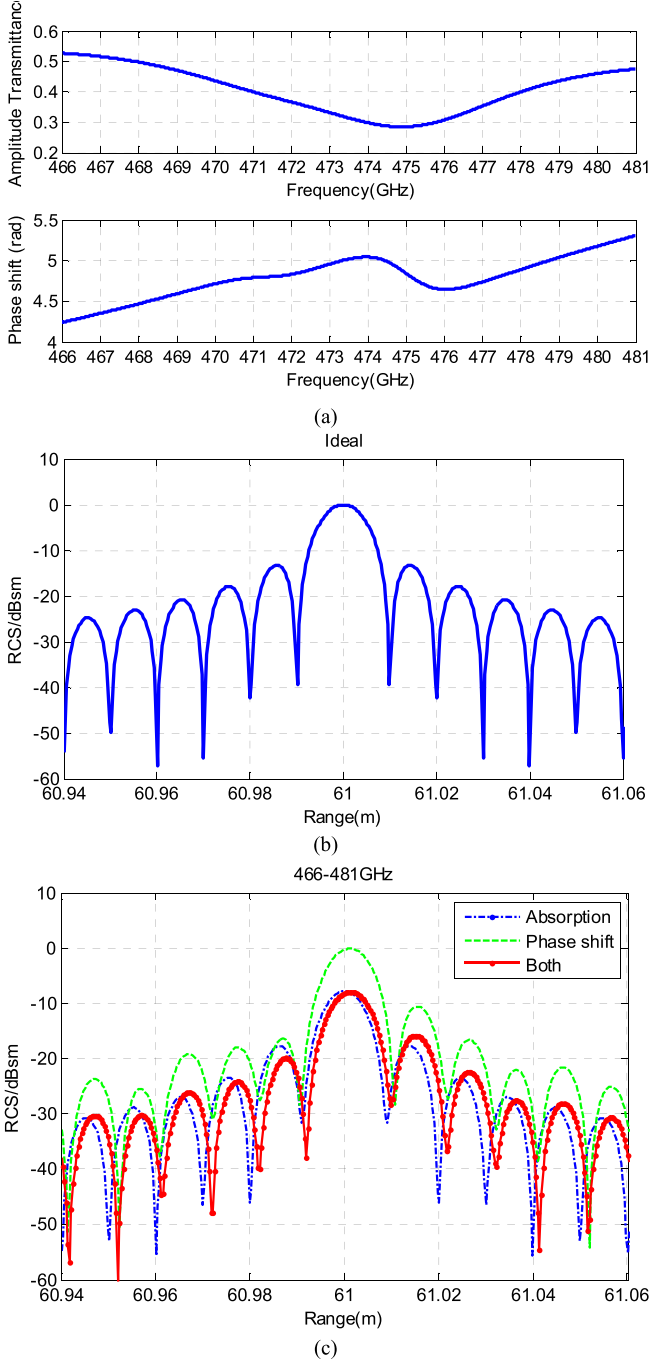


Fig. 4. Simulated range profiles at frequency spanning from 466 to 481 GHz. (a) Amplitude transmittance and phase shift through 122 m of atmosphere. (b) Ideal. (c) Distorted range profiles, where the blue solid curve, the green dashed curve, and the red curve with dots represent the results considering only attenuation, only phase shift, and both attenuation and phase shift, respectively.

When both the attenuation and the phase shift are considered, the range profile is presented as the red curve with dots shown in Fig. 4(c). In terms of the paired echoes [25], the amplitude and phase distortions correspond to the positive and the negative pairs, respectively. The positive and negative pairs before the expected signal offset each other leading to a decrease in the intensity of the sidelobes, whereas the positive and negative pairs after the main lobe enhance the sidelobes.

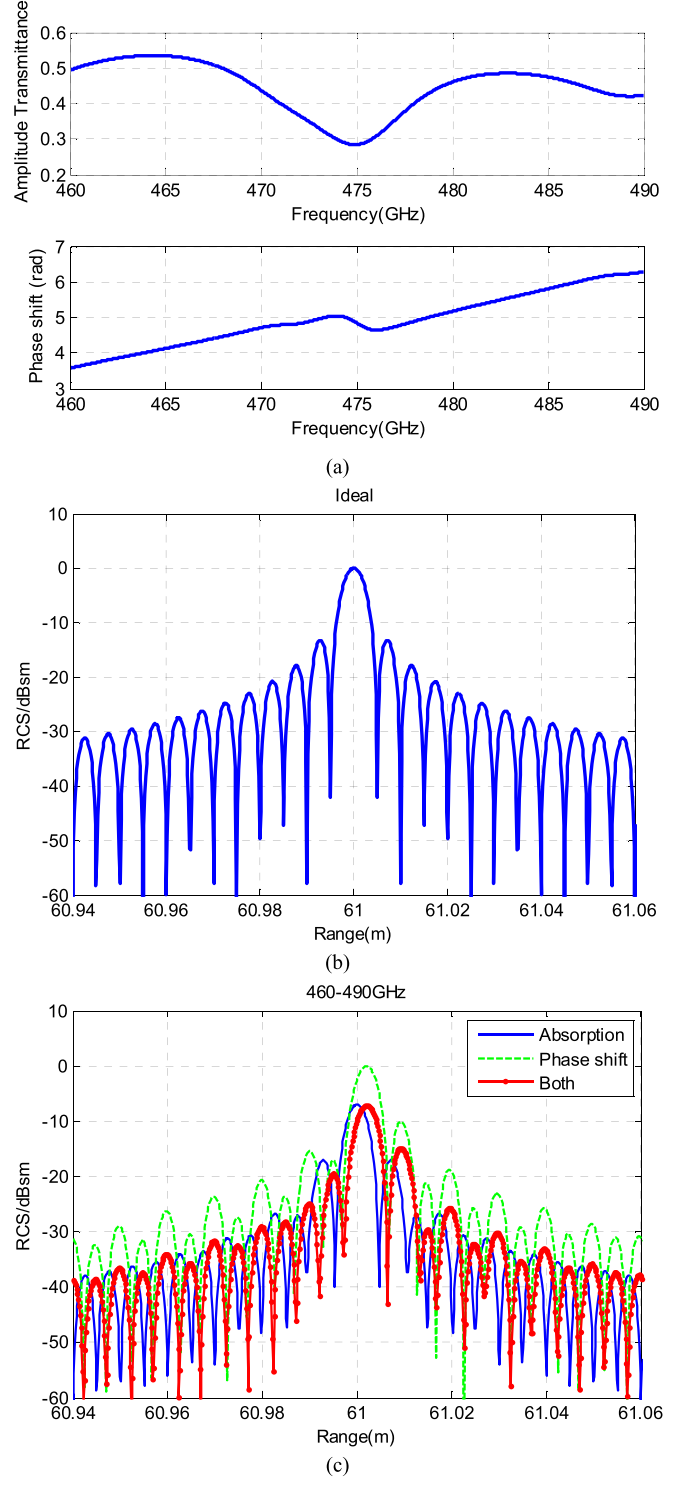


Fig. 5. Simulated range profiles at frequency spanning from 460 to 490 GHz. (a) Atmospheric transfer characteristics. (b) Ideal. (c) Distorted range profiles, where the blue solid curve, the green dashed curve, and the red curve with dots represent the results considering only attenuation, only phase shift, and both attenuation and phase shift, respectively.

As shown by the red curve in Fig. 4(c), the secondary peak of the range profile is approximately 7.9 dB lower than the main peak. In contrast, the sidelobes of the ideal signal proceeded with a rectangular window are about -13 dB, as shown in Fig. 4(b).

To achieve a higher resolution, a wider bandwidth should be adopted. However, the wideband signal can be easily impacted by the atmospheric attenuation and phase shift. As an example, the frequency channel covering 460–490 GHz is used to simulate the range profiles, while other parameters are kept the same. The results are presented in Fig. 5.

Compared to Fig. 4, the atmospheric transfer attenuation is similar, whereas the width of the main lobe shown in Fig. 5 is much narrower indicating a higher resolution. However, similar to Fig. 4(c), the range profiles shown in Fig. 5(c) are remarkably distorted. Since the nonlinear amplitude attenuation is as severe as that in the frequency channel from 466 to 481 GHz, positive pairs of echoes can be found, while the second peak is 10.08 dB lower than that of the main peak. In addition, with a higher resolution, the location shift of the scattering center is clearly shown in Fig. 5(c).

As it can be seen in the analyses, THz frequencies can provide the wide bandwidth for radar imaging to obtain high-resolution range profiles. However, the signal after atmospheric transfer will be distorted by the inconstant attenuation and the nonlinear phase shift in the specific frequency channel, especially for long-distance imaging. Thus, the frequency channel for radar imaging should be selected carefully, while a compromise between imaging quality and resolution should be considered in the development of THz radar systems.

IV. CONCLUSION

The physics-based prediction of the transmittance and phase shift caused by atmospheric gases is implemented to simulate radar imagery at THz frequencies in this paper. To this end, the line-by-line calculation method is adopted with the specific modification in phase-shift prediction. The line-by-line spectroscopic parameters are provided by the HITRAN, while the AFGL reference atmospheric constituent profiles are used to simulate specific atmospheric conditions.

The calculated amplitude transmittance and phase shift are, respectively, compared with measured data to demonstrate the accuracy. Although only the spectral lines of water vapor are used in the calculation, the obtained curves of transmittance and phase shift have negligible difference from the measured data, especially in the spectrum ranging from 0.2 to 1 THz. In addition, the proposed procedure is used in the high-resolution range profile simulation to analyze the impacts of atmospheric transmittance and phase shift on THz radar imagery. The simulated range profiles show different kinds of signal distortions, including magnitude attenuation, location shift of the scattering centers, and artifacts generated from paired echoes. These results demonstrate the importance of frequency channel selection in the development of THz radar systems, especially for long-distance detection and imagery.

REFERENCES

- [1] P. H. Siegel, “THz instruments for space,” *IEEE Trans. Antennas Propag.*, vol. 55, no. 11, pp. 2957–2965, Nov. 2007.
- [2] J. F. Federici, “THz imaging and sensing for security applications—explosives, weapons and drugs,” *Semicond. Sci. Technol.*, vol. 20, no. 7, pp. S266–S280, Jun. 2005.
- [3] S. Priebe, C. Jastrow, M. Jacob, T. Kleine-Ostmann, T. Schrader, and T. Kurner, “Channel and propagation measurements at 300 GHz,” *IEEE Trans. Antennas Propag.*, vol. 59, no. 5, pp. 1688–1698, May 2011.
- [4] H. Balacey, B. Recur, J.-B. Perraud, J. B. Sleiman, J.-P. Guillet, and P. Mounaix, “Advanced processing sequence for 3-D THz imaging,” *IEEE Trans. THz Sci. Technol.*, vol. 6, no. 2, pp. 191–198, Mar. 2016.
- [5] R. Appleby and H. B. Wallace, “Standoff detection of weapons and contraband in the 100 GHz to 1 THz region,” *IEEE Trans. Antennas Propag.*, vol. 55, no. 11, pp. 2944–2956, Nov. 2007.
- [6] A. A. Danylov *et al.*, “Terahertz inverse synthetic aperture radar (ISAR) imaging with a quantum cascade laser transmitter,” *Opt. Express*, vol. 18, no. 15, pp. 16264–16272, Jul. 2010.
- [7] K. B. Cooper, R. J. Dengler, N. Llombart, B. Thomas, G. Chattopadhyay, and P. H. Siegel, “THz imaging radar for standoff personnel screening,” *IEEE Trans. THz Sci. Technol.*, vol. 1, no. 1, pp. 169–182, Sep. 2011.
- [8] M. Kowalski and M. Kastek, “Comparative studies of passive imaging in Terahertz and mid-wavelength infrared ranges for object detection,” *IEEE Trans. Inf. Forensics Security*, vol. 11, no. 9, pp. 2028–2035, Sep. 2016.
- [9] *Attenuation by Atmospheric Gases*, document ITU-R P.676-11, Sep. 2016.
- [10] *Specific Attenuation Model for Rain for use in Prediction Methods*, document ITU-R P.838-3, 2005.
- [11] *Attenuation due to Clouds and Fog*, document ITU-R P.840-5, Feb. 2012.
- [12] Y. Yang, A. Shutler, and D. Grischkowsky, “Measurement of the transmission of the atmosphere from 0.2 to 2 THz,” *Opt. Express*, vol. 19, no. 9, pp. 8830–8838, Apr. 2011.
- [13] Y. Yang, M. Mandehgar, and D. R. Grischkowsky, “Understanding THz pulse propagation in the atmosphere,” *IEEE Trans. THz Sci. Technol.*, vol. 2, no. 4, pp. 406–415, Jul. 2012.
- [14] G. P. Anderson, J. H. Chetwynd, S. A. Clough, E. P. Shettle, and F. X. Kneizys, “AFGL atmospheric constituent profiles (0.120 km),” AFGL, Hanscom AFB, MA, USA, Tech. Rep. AFGL-TR-86-0110, May 1986.
- [15] S. A. Clough *et al.*, “Atmospheric radiative transfer modeling: A summary of the AER codes,” *J. Quantitative Spectrosc. Radiat. Transfer*, vol. 91, no. 2, pp. 233–244, Mar. 2005.
- [16] A. Berk, L. S. Bernstein, and D. C. Robertson, “MODTRAN: A moderate resolution model for Lowtran,” AFGL, Hanscom AFB, MA, USA, Tech. Rep. AFGL-TR-87-0220, Jul. 1987.
- [17] P. Ricchiazzi, S. Yang, C. Gautier, and D. Sowle, “SBDART: A research and teaching software tool for plane-parallel radiative transfer in the earth’s atmosphere,” *Bull. Amer. Meteorol. Soc.*, vol. 79, no. 10, pp. 2101–2114, Oct. 1998.
- [18] C. J. Willers, *Electro-optical System Analysis and Design: A Radiometry Perspective*. Bellingham, WA USA: SPIE, 2013.
- [19] L. S. Rothman *et al.*, “The HITRAN molecular spectroscopic database and hawks (HITRAN atmospheric workstation): 1996 edition,” *J. Quant. Spectrosc. Radiat. Transfer*, vol. 60, no. 5, pp. 665–710, 1998.
- [20] L. S. Rothman *et al.*, “The HITRAN2012 molecular spectroscopic database,” *J. Quant. Spectrosc. Radiat. Transfer*, vol. 130, pp. 4–50, Nov. 2013.
- [21] R. M. Goody, “A statistical model for water-vapour absorption,” *Quart. J. Roy. Meteorol. Soc.*, vol. 78, pp. 638–640, Oct. 1952.
- [22] W. L. Godson, “The evaluation of infra-red radiative fluxes due to atmospheric water vapour,” *Quart. J. Roy. Meteorol. Soc.*, vol. 79, pp. 367–379, Jul. 1953.
- [23] R. J. Hill, “Water vapor-absorption line shape comparison using the 22 GHz line: The Van Vleck–Weisskopf shape affirmed,” *Radio Sci.*, vol. 21, no. 3, pp. 447–451, May 1986.
- [24] C. H. Townes and A. I. Schawlow, *Microwave Spectroscopy*. New York, NY, USA: Dover, 1975.
- [25] H. A. Wheeler, “The interpretation of amplitude and phase distortion in terms of paired echoes,” *Proc. IRE*, vol. 27, no. 6, pp. 359–384, Jun. 1939.

Authors’ photographs and biographies not available at the time of publication.